A Feasibilty Study on Detection of Neovascularization in Retinal Color images Using Texture

Maryam Vatanparast
Computer Engineering Department
Faculty of Eng., Ferdowsi University of Mashhad
Mashhad, Iran
E-mail: maryam.vatanparast@stu-mail.um.ac.ir

Ahad Harati
Computer Engineering Department
Faculty of Eng., Ferdowsi University of Mashhad
Mashhad, Iran
E-mail: a.harati@um.ac.ir

Abstract— **Retinal Neovascularization (NV) is one of the most important causes of diabetic blindness which emphasizes the serious need for automatic screening tools to diagnose diabetes and treat it as early as possible. In this work, the problem of NV detection in the color images of retina is considered.**

Previous researches in the analysis of retinal images either ignore such complex lesion or in few cases approach it superficially and pose many limitations. Obtaining a complete vessel map and then trying to identify NV is a recent methodology. Unfortunately, NV mainly affects small and hard to detect vessels, hence, we believe such an approach is inherently limited. Therefore, in this paper six different texture descriptions are proposed as features in the classification of retinal images into NV and normal group. We study application of the proposed features using a support vector machine (SVM) as a simple classifier to emphasize the importance of features against the complexity of the classifier. Feature extraction is performed on local regions of the images (128x128) to localize the lesion.

A dataset of 1613 regions is considered that contains 591 NV regions which are manually marked by an expert. The results show the proposed texture descriptors are able to reveal the NV lesion with an acceptable accuracy of around 90%.

Keywords- Neovascularization; Retinal image analysis; texture analysis algorithms

I. INTRODUCTION

Importance of early diagnosis of diabetes based on analysis of retinal images is increasing more and more as this disease is affecting more number of people every day. Diabetic retinopathy (DR) has a fundamental role in visual impairment in the world. Retinal Neovascularization is one of the most important causes of DR related blindness [1]. In order to have an early detection of DR, a periodical screening procedure is highly advised. This demands automatic detection algorithms for different stages of DR; among them NV is one the most critical and challenging lesions for classification.

Color fundus images are frequently used in such screenings. Little researches have been carried out on detection of NV, which can be classified in two categories. In initial efforts, the proliferative diabetic retinopathy (PDR) is differentiated from the other stages of DR [2-4]. In [2, 4] a supervised learning method is applied to recognize different stages of the DR. Morphological operations is used for feature extraction from RGB planes. Four types of retinal defections are classified by backward neural network using fuzzy c-means in [3]. In advanced activities NV is detected as a lesion in PDR stage [5-8]. Two texture based methods [5, 6] have been proposed in 1997 and 2010 respectively. In [5] first order and second order statistics texture features are measured and Linear Discriminant Analysis is performed for classification of NV and Exudate. In [6] texture features are computed by AM-FM transform and a linear regression method, partial least square (PLS), is applied to recognize the four different stages of DR. In addition, Mahalanobis metric is calculated between different lesions and investigates the distinction capability of extracted features. [7] shows that various combination of techniques such as image normalization, compactness classifier, morphology-based operator etc. are used in detection of NV; utilizing vessel extraction procedure and defining two assumptions would be effective for developing a region-based method. The approach developed in [8] is detecting new vessels on the optic disc. Vessel-like candidate segments are first detected using a method based on watershed lines and ridge strength measurement. Feature parameters are calculated for each candidate segment. Based on these features, each segment is categorized as normal or abnormal using a SVM classifier.

Since the vessels are in the different sizes and the neovessels are frequently found in very small sizes and also most of the vessel detection algorithms cannot be that much exact to extract nearly all of the tiny vessels, it results that extracting the vessel maps and extracting different features for them is not adequate. Therefore we suppose the vessel structures to have textural information and without considering the vessel maps and tracking them, detect NV by extracting texture features from the image.

Nevertheless little researches have been performed in detection of NV; proper feature set is not established. Thus we focus on the extraction of features rather than choosing classifier.

As there are no public databases which are labeled as NV, by one or more medical specialist, there would be a fundamental problem with retinal databases in comparison between different publications of this research. As a beginning of publishing NV-labeled retinal databases we are interested to make our labeled database available to retinal researchers. Because the rate of progression of DR and specially PDR stage depend on the geometrical locality, the negative effect of absence of public database is partly reduced.

Our aim is to highlight the areas of images containing NV lesion, and the system that will be developed in this research is just an advertisement system which tries to differentiate normal regions with more accuracy.

The preliminary information about the research, related researches in NV detection and the main contribution was described in section I. The background of texture analysis and the selected algorithms are defined in section II. Section III, database and preparation of the methods are explained. And the results are shown in section IV. Finally in section V the conclusion and what would be done in future are noted.

II. BACKGROUND

A. Texture Analysis

There are different approaches to extract textural features for analyzing textural information in the image, e.g. multi-resolution analysis [9, 10], local pattern spectrum [11] and co-occurrence of gray scale values [12] to texel (texture unit) spectrum- based approaches [13]. Gabor filter-based approaches [14-16], wavelet transform [17, 18] and Gaussian Markov random field (MRF) [19, 20] are the most favorite techniques for analyzing texture.

As mentioned in [21] there are two general categories for texture classification methods. The first group is spatial-domain methods which are divided into three subcategories, structural methods, statistical methods and model-based methods. These kinds of methods are restricted to the analysis of spatial interactions over relatively small neighborhoods. Therefore, their performances are only good for the class of so-called micro-textures. To alleviate these essential problems of spatial-domain methods, transformed-domain methods have been proposed from a different point of view.

For the preliminary of this research we propose six texture-based methods and compare the accuracy and efficiency of them. Two of the methods applied in this work have been introduced in this domain (Grey Level Co-occurrence Matrix and Amplitude Modulation-Frequency Modulation).

Due to the structure of vessels that are oriented, the approaches which extract textural features in different directions would be appropriate in this research. Gabor and Contourlet transforms are multi-scale and multi-direction which can describe the texture of NV properly.

LBP is another texture approach that can describe non-specified textures.

B. Selected Texture Analysis Methods

1) Grey Level Co-occurrence Matrix: GLCM [22] is a tabulation of how often different combinations of pixel brightness values (grey levels) occur in a predefiened relative position in an image. Considering an $n \times m$ image I with G gray scale values and parameterized with an offset $(\Delta x, \Delta y)$, the GLCM is a $G \times G$ matrix which it's (i,j)th element represents the count of co-occurrence of values i and j in the specified scale and orientation. Using the co-occurrence matrix for different scales and orientations, results different features. The features that are used included: energy, entropy, contrast, correlation and etc as mentioned in [23-25]. There are two problems with using the GLCM. The first is in choosing the appropriate scale and orientation parameters to obtain the structural information of the texture in the obtimal way, and for the other problem, high computation complexity can be noted.

2) Gabor Filters: In the spatial domain, a 2D Gabor filter is a Gaussian kernel function modulated by a sinusoidal plane wave. The 2-D Gabor wavelet is defined as

$$\varphi_G(x,y) = \exp(jK_0(1)srX + jK_0(2)srY) * G(x,y) \quad (1)$$

$$\mathrm{srX} = \mathrm{x/a}\ \cos(-\theta) - \mathrm{y/a}\ \sin(-\theta), \quad (2)$$

$$\mathrm{srY} = \mathrm{x/a}\ \cos(-\theta) + \mathrm{y/a\ si\ n}(-\theta), \quad (3)$$

$$\mathrm{G(x,y)} = \exp\left(-\frac{1}{2}((\mathrm{srX} * \varepsilon^{-\frac{1}{2}})^2 + (\mathrm{srY})^2\right)). \quad (4)$$

The Gabor wavelet is a complex exponential modulated Gaussian, $G(x,y)$, where $K_\circ$ is a vector that defines the frequency of the complex exponential and srX and srY are the scaled and rotated coordinates [26]. In this work, we have used 5 scales (denoted as a) and 18 orientations (denoted as θ) and then set the ε parameter to 4, making the filter elongated and $K_\circ = [0, 3]$, i.e., the horizontal and vertical frequencies. A detailed description for computing Gabor filters responses can be found in [26].

3) Amplitude Modulation-Frequency Modulation: Image $I(x,y)$ can be approximated by a sum of AM-FM components as formulated in (5).

$$\mathrm{I(x,y)} \approx \sum_{n=1}^{M} \mathrm{a_n(x,y)cos\varphi_n(x,y)}, \quad (5)$$

where M is the number of AM-FM components. a and φ functions are considered as instantaneous amplitude (IA) and instantaneous phase functions, respectively [27]. There is an implementation for this method in based on DFBs which has 9 combinations related to 4 scales and 25 band-

pass channel filters. In this paper, due to availability of a toolbox for decomposing image into channels based on steerable pyramid, we use the implementation introduced in [28]. This transform decompose image into 40 channels and demodulate channels into 3 estimates. Instantaneous amplitude, instantaneous frequency and instantaneous phase are the computed estimates. Instantaneous frequency is calculated in terms of the gradient phase as in (6).

$$\nabla_{\varphi_n}(x,y) = \left(\frac{\delta_{\varphi_n}(x,y)}{\delta_x}, \frac{\delta_{\varphi_n}(x,y)}{\partial_y}\right). \quad (6)$$

We can refer to [29] for more details about this decomposition. Here the focus is on the feature extraction. We use the same estimates that are specified in [6, 30] as textural features (IA, |IF| and IF relative angles). Although there are basic similarities to the approach proposed in [30], we describe the fundamental procedure to compute the main features. The channels are combined to simulate five scales with regards to their frequency (TABLE I). TABLE II describes 9 combinations of channels that has been selected based on the rules in [30]. In each combination of scales (CoSs) we use dominant component analysis (DCA) to choose the dominant channel (TABLE II). Since the CoSs obtained, we calculate Mahalanobis distance for the CDFs of each CoS per estimates between mean of normal and abnormal regions as discussed in [6]. To check the accuracy of the implemented algorithm a test is performed using Mahalanobis distance. In this paper, the concept of AM-FM would be the one which uses steerable pyramid.

4) Contourlet Transform: To eliminate the limitations of wavelet transform, the contourlet transform has been developed [31]. In fact it would be better wavelet transform to capture the curves in an image . The structure of this transform includes the laplasian pyramid (LP) and a directional filter bank (DFB). Because of this cascading structure, multiscale and directional decomposition stages are independent of each other. Thus we are capable to decompose each scale into any power of tow directions and each scale can be decomposed into different number of directions. Through using discrete contourlet transform, an image can be decomposed into a set of coefficients introduced in (7).

$$C_{i,j}^{(l_i)}[n], \quad i = 1, 2, \dots, I \text{ and } j = 0, 1, \dots, 2^{l_i} - 1 \quad (7)$$

The indices *i, j* and n denote to scale, direction and location, respectively. The number of DFB decomposition levels is l_i and I specify the highest LP decomposition. In this paper, the number of levels is 3 and l_i for each level is 2. Thus the image is decomposed into a low-pass subband and 12 band-pass directional subbands.

TABLE I
BANDPASS FILTERS ASSOCIATED WITH MULTIPLE IMAGE SCALES

Frequency scale band	Combined channels	Named as
Low Pass Filter (LPF)	Channels 33:40	Channel 1
Very Low frequencies (VL)	Channels 25:32	Channels 26:33
Low Frequencies (L)	Channels 17:24	Channels 18:25
Medium Frequencies (M)	Channels 9:16	Channels 10:17
High Frequencies (H)	Channels 1:8	Channels 2:9

TABLE II
COMBINATION OF SCALES

Combination Number	Channels	Frequency Bands
1	1:33	M + L + VL
2	1	LPF
3	26:33	VL
4	18:25	L
5	10:17	M
6	18:33	L + VL
7	10:25	M + L
8	2:9	H
9	2:17	H + M

5) Local Binary Pattern: LBP has since been found to be a powerful feature for texture classification. In general, a binary code for each pixel of an image is produced by thresholding the n × n pixels in neighborhood of the specified pixel using the value of the centered pixel. The feature vector to describe the textural information of the specified pixel is the histogram of the assigned indices. To encode the different scale variations LBP can be extended to multiple scales.we can use bilinear interpolating to extend the size of circular neighborhood. There are two parameter to describe the LBP code (R and SP). R is the radious and SP is the number of sampling points that are considered in circular neighborhood. The LBP code is shift invariant, since the gray value at the center of the pixel is subtracted from the gray values of its circular neighborhood. In this work, we use LBP computed from three different scales [1, 2 and 3].

6) Rotation Invariant LBP: There are two important variations of LBP, LBP with uniform patterns and LBP with rotation invariance. The binary patterns with only two transitions (from 0 to 1 and vice versa) are uniform patterns. It was also suggested in [32] that by performing circular bit-wise right shift on the SP-bit number, rotation invarient LBP can be obtained.

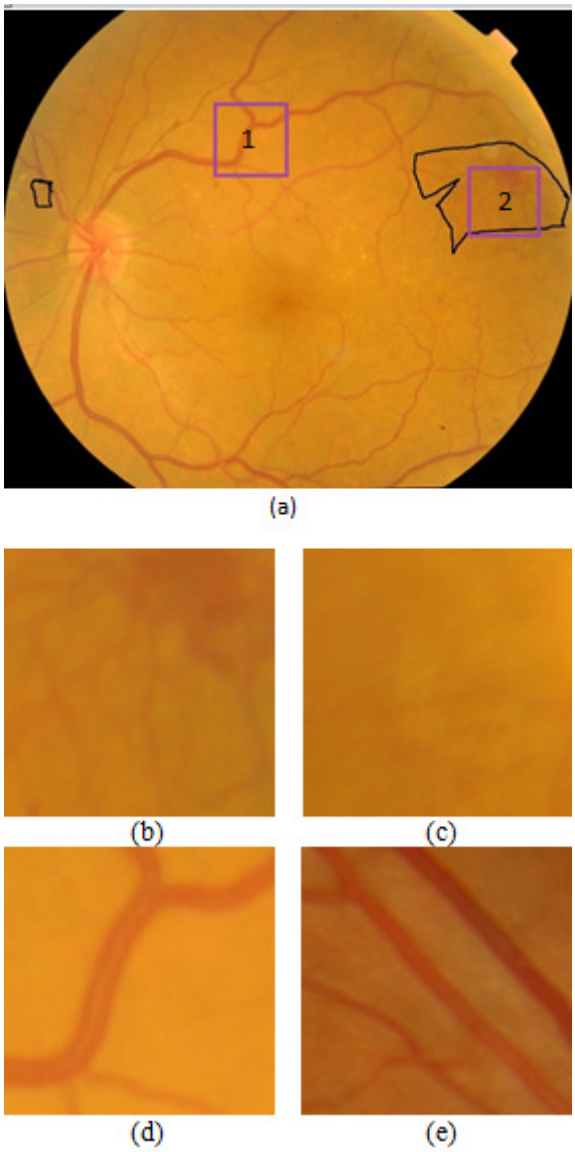

Fig. 1. (a) Image from KHPDR database. Lesions encased in the boxes are examples of: (1) NV and (2) Normal. (b) and (c) are the examples of NV region. (d) and (e) are the examples of normal region.

III. DATABASES AND EXPERIMENTAL SETUP

A. *Databases*

To assess performance of the proposed methods, fundus images from a local database, KHPDR[1], specifically created for this work is used. KHPDR is currently under development and will be freely available to researchers as soon as it is ready for public use.

Among the studied methods, AM-FM has to work with sub-images which have rows and columns that are power of two. Therefore, size of local window is set to 128x128.

Custom labeling software used for the labeling of the databases by the medical expert. Since large portion of the implementations used for feature extraction in this work are still research codes and not optimized for speed; KHPDR images are down sampled to 0.47 to improve execution time.

In this paper, 31 abnormal images which have areas with NV lesions along with 12 normal images are selected form KHPDR. The images of this database are in PNG format (3872x2592 pixels). Images of this database have a high resolution, but the NV lesion in some areas is not enough well-known, e.g. in Fig. 1(c) the NV lesion is not obvious.

B. *Feature Extraction*

In this work, the focus is on the extracting texture features. As NV has a multi-resolution property, so we require checking large and small resolutions. As regards the characteristics of Neovascularization, each method should be parameterized in such a way that the multi-scale property is established. Also because of the abundance of features extracted for each region in certain methods, PCA [2] performed on feature vectors to reduce the dimensionality.

In GLCM, for any region, 3 distances and 4 symmetric directions are used to extract 18 features form each distance per direction. Eventually, a feature vector with 216 dimensions produced and reduced to 14 by choosing 99 percentage of energy.

In the case of Gabor, Maximum of 18 directions from each of 5 image scales is used. Five features (Mean, Variance, Skewness, Kurtosis and Energy) were computed from Gabor coefficients in different scales. So the number of extracted features will be 25.

In Contourlet method, 3 levels and 4 directions for each level are selected. The maximum direction is then picked out from each level. Five features as mention in Gabor case are computed for levels and even the low-pass subband. Finally 20 features produced for each region.

As mentioned in section II. B. 3, three CDFs of estimates for any of the nine CoSs are calculated in AM-FM. Therefore there would be 27 CDFs with 40 bins as feature vectors (Totally each region has 1080 features). In the procedure of decomposition and combination of channels there are so much redundancy, so the whole 27 CDFs and bins are not required. Therefore PCA is performed on the feature vectors for each estimate per CoS. By analyzing the proper number of bins after PCA, there would be an efficient number of bins for each of 27 CDFs (Average number of bins is 3). In this paper, the CDFs are sorted based on the maximum Mahalanobis distance and the accuracy of the algorithm is tested for different number of selected CDFs, then we conclude that the appropriate number of selected CDFs is 8. Thus the number of features is almost 24 (8×3).

[1] Khatam Alanbia Hospital Proliferative Diabetic Retinopathy - Images are provided from a local hospital in Mashhad.

[2] Principle Component Analysis

TABLE III
COMPARISON OF ACCURACY OF PROPOSED METHODS USING KHPDR DATABASE

	GLCM	Gabor	AMFM	Contourlet	LBP	LBP (RI)
TP	82	113	101	109	102	95
TN	197	191	194	183	196	194
FP	36	5	17	9	16	23
FN	7	13	10	21	8	10
SN	92.13	89.68	90.99	83.85	92.73	90.48
SP	84.55	97.45	91.94	95.31	92.45	89.40

TABLE IV
RUNNING TIME OF FEATURE EXTRACTION FOR EACH METHOD (Region per Second)

	GLCM	Gabor	AMFM	Contourlet	LBP	LBP (RI)
F.E.	1.15	4.19	23.33	13	0.03	0.01

TABLE V
DIFFERENT VALUES OF THE PARAMETER C OF SVM CLASSIFIER FOR EACH OF THE METHODS

	GLCM	Gabor	AMFM	Contourlet	LBP	LBP (RI)
C	0.002	10	1	0.002	0.5	10

In the uniform form of LBP, three distances [1, 2 and 3] as different scales and for each of the scales eight sample points in neighborhood of the centered pixel are chosen. The output of the algorithm is an image which contains the LBP codes for each pixel. Five features for each scales are computed, the same as the ones in Gabor, and the final feature vector has 15 dimensions.

Rotational Invariant LBP parameters are set like the LBP but the outputs are histograms for each scale which are the histograms of the image that contains LBP codes. PCA is performed on the merged array of histograms of all scales to reduce the dimensions. Then 95 percentage of energy is taken and five features are calculated from the left 34 dimensions. Totally five features is produced for each of the regions.

C. Classification

As mentioned above in this work, the focus was on the extracting features, rather than the impact of the classifier. As long as the features were extracted, a rather powerful classifier was chosen to separate Neovascularization regions from normal regions. In order to compare the performance of mentioned methods, the SVM with linear kernel was applied. In this paper, the parameter C of SVM classifier is tested for different feasible values, and is set for each of the six methods separately. In TABLE V the value of the parameter C is reported for each method.

IV. EXPERIMENTAL RESULTS AND DISCUSSION

A. Results

322 regions randomly applied for test. The algorithms are compared by the values, True Positive, True Negative, False Positive, False Negative, Sensitivity and Specificity. In TABLE III the performance of the implemented methods using KHPDR database are listed.

In TABLE IV the time which is consumed for feature extraction and classification of 1613 regions for each of methods using SVM are reported.

B. Discussion

In this paper the main idea is checking the feasibility of detection of NV using different texture methods so we are not considering optimizing the parameters of the classifier. Although if the parameters of the classifier is set to optimum, the results would be more accurate. Our purpose is to study the quality of the extracted texture features in an equal condition of classification.

The results in TABLE III demonstrate that all the methods have a proper performance and are feasible for using as a texture descriptor in this area of research.

There is not that much difference between the results, the rotation invariant method has better sensitivity and the specificity of Gabor method is the maximum.

V. CONCLUSION AND FUTURE WORK

Detection of neovascularization is a difficult task for retinal abnormality detection. As NV is a complex lesion and is in the latest stages of DR, little researches were carried out in detection of it. We considered that texture information which can be extracted from image would be appropriate to detect NV lesion. In this paper we showed that we can use texture descriptors such as Gabor, GLCM etc. to differentiate NV regions from normal regions. In fact without using a vessel map the NV lesion is detected with an acceptable accuracy.

In future these methods will be compared in their error regions and combination of two or more of the texture methods may be effective to improve the accuracy.

REFERENCES

[1] A. Das, "Human Diabetic Neovascular Membranes Contain High Levels of Urokinase and Metalloproteinase Enzymes," 1999.

[2] W. L. Yun, et al., "Identification of different stages of diabetic retinopathy using retinal optical images," Information Sciences, vol. 178, pp. 106-121, 2008.

[3] J. Anitha, et al., "Neural Computing Based Abnormality Detection in Retinal Optical Images," in Advance Computing Conference, 2009. IACC 2009. IEEE International, 2009, pp. 630-635.

[4] U. R. Acharya, et al., Computer-based detection of diabetes retinopathy stages using digital fundus images vol. 223, 2009.

[5] A. J. Frame, et al., "Texture analysis of retinal neovascularisation," in Pattern Recognition (Digest No. 1997/018), IEE Colloquium on, 1997, pp. 5/1-5/6.

[6] C. Agurto, et al., "Multiscale AM-FM Methods for Diabetic Retinopathy Lesion Detection," Medical Imaging, IEEE Transactions on, vol. 29, pp. 502-512, 2010.

[7] C. Agurto, et al., "Multiscale AM-FM Methods for Diabetic Retinopathy Lesion Detection," Medical Imaging, IEEE Transactions on, vol. 29, pp. 502-512, 2010.

[8] K. A. Goatman, et al., "Detection of New Vessels on the Optic Disc Using Retinal Photographs," Medical Imaging, IEEE Transactions on, vol. 30, pp. 972-979, 2011.

[9] M. Unser and M. Eden, "Multiresolution Feature Extraction and Selection for Texture Segmentation," IEEE Trans. Pattern Anal. Mach. Intell., vol. 11, pp. 717-728, 1989.

[10] J. Mao and A. K. Jain, "Texture classification and segmentation using multiresolution simultaneous autoregressive models," Pattern Recogn., vol. 25, pp. 173-188, 1992.

[11] P. Maragos, "Pattern spectrum and multiscale shape representation," IEEE Transactions on Pattern Analysis and Machine Intelligence, vol. 11, pp. 701-716, 1989.

[12] L. S. Davis, et al., "Texture Analysis Using Generalized Co-Occurrence Matrices," IEEE Trans. Pattern Anal. Mach. Intell., vol. 1, pp. 251-259, 1979.

[13] L. Wang and D.-C. He, "Texture classification using texture spectrum," Pattern Recogn., vol. 23, pp. 905-910, 1990.

[14] B. S. Manjunath and W. Y. Ma, "Texture features for browsing and retrieval of image data," Pattern Analysis and Machine Intelligence, IEEE Transactions on, vol. 18, pp. 837-842, 1996.

[15] A. C. Bovik, et al., "Multichannel Texture Analysis Using Localized Spatial Filters," IEEE Trans. Pattern Anal. Mach. Intell., vol. 12, pp. 55-73, 1990.

[16] A. K. Jain and F. Farrokhnia, "Unsupervised texture segmentation using Gabor filters," Pattern Recogn., vol. 24, pp. 1167-1186, 1991.

[17] A. Laine and J. Fan, "Texture Classification by Wavelet Packet Signatures," IEEE Trans. Pattern Anal. Mach. Intell., vol. 15, pp. 1186-1191, 1993.

[18] S. C. Kim and T. J. Kang, "Texture classification and segmentation using wavelet packet frame and Gaussian mixture model," Pattern Recogn., vol. 40, pp. 1207-1221, 2007.

[19] R. W. Conners and C. A. Harlow, "A Theoretical Comparison of Texture Algorithms," IEEE Trans. Pattern Anal. Mach. Intell., vol. 2, pp. 204-222, 1980.

[20] A. Rangarajan and R. Chellappa, "Markov random field models in image processing," in The handbook of brain theory and neural networks, A. A. Michael, Ed., ed: MIT Press, 1998, pp. 564-567.

[21] Y. Dong and J. Ma, "Bayesian Texture Classification Based on <newline/>Contourlet Transform and BYY Harmony<newline/> Learning of Poisson Mixtures," Image Processing, IEEE Transactions on, vol. 21, pp. 909-918, 2012.

[22] R. M. Haralick, "Statistical and structural approaches to texture," Proceedings of the IEEE, vol. 67, pp. 786-804, 1979.

[23] K. S. Robert M. Haralick, and Its'hak Dinstein, "Textural Features for Image Classification," IEEE Transaction on Systems, Man and Cybernetics, vol. SMC-3, NO. 6, pp. 610-621, November 1973.

[24] D. A. Clausi, "An analysis of co-occurrence texture statistics as a function of grey level quantization," Canadian Journal of Remote Sensing, vol. 28, 2002.

[25] L. Soh and C. Tsatsoulis, "{Texture Analysis of SAR Sea Ice Imagery Using Gray Level Co-occurrence Matrices}," IEEE Trans. Geosci. Remote Sensing, vol. 37, pp. 780-795, 1999.

[26] J. V. B. Soares, et al., "Retinal vessel segmentation using the 2-D Gabor wavelet and supervised classification," Medical Imaging, IEEE Transactions on, vol. 25, pp. 1214-1222, 2006.

[27] M. S. Pattichis and A. C. Bovik, "Analyzing Image Structure by Multidimensional Frequency Modulation," IEEE Trans. Pattern Anal. Mach. Intell., vol. 29, pp. 753-766, 2007.

[28] Available: http://amfm.ou.edu/

[29] J. P. Havlicek, et al., The multicomponent AM-FM image representation vol. 5, 1996.

[30] V. Murray, "AM-FM methods for image and video processing," Ph.D., Albuquerque, New Mexico, Sep. 2008.

[31] M. N. Do and M. Vetterli, "The contourlet transform: an efficient directional multiresolution image representation," Image Processing, IEEE Transactions on, vol. 14, pp. 2091-2106, 2005.

[32] T. Ojala, et al., "Multiresolution Gray-Scale and Rotation Invariant Texture Classification with Local Binary Patterns," Pattern Analysis and Machine Intelligence, IEEE Transactions on, vol. 24, pp. 971-987, 2002.